remote sensing

MDPI

Editorial

Advances in InSAR Imaging and Data Processing—A Review

Lei Zhang [1] and Zhong Lu [2,*]

[1] College of Surveying and Geo-Informatics, Tongji University, No. 1239 Siping Rd., Shanghai 200092, China
[2] Huffington Department of Earth Sciences, Southern Methodist University, Dallas, TX 75275, USA
* Correspondence: zhonglu@smu.edu

1. Introduction

Through different phases of synthetic aperture radar (SAR) data acquired on different dates and/or at different satellite imaging locations, the interferometric SAR (InSAR) technique has long been used to map ground deformation or generate global digital elevation model (DEM) (e.g., [1–3]). Provided that deformation mapping is the signal of interest, external DEM can be used to estimate the phases raised by topographic heights according to the SAR imaging geometry. It is obvious that when the external DEM is not accurate, the induced error will remain in the InSAR phases, degrading the accuracy of the retrieved deformation. In addition, the accuracy of InSAR-derived deformation maps can also be affected by decorrelation noise, atmospheric artefact, orbit uncertainty, and phase unwrapping error among others. The recent development of multi-temporal InSAR (MTInSAR) techniques deals with mitigating these unwanted phase components (e.g., [4]). The pioneering works include, but are not limited to, the derivation of statistical properties of magnitude and phase of both distributed and persistent scatterers under the assumption that the backscattered signal of a resolution cell follows complex circular Gaussian distribution [5–7], the maximum likelihood estimation of the interferometric phase [8], the probability density function of multilook data [9,10], the phase decorrelation mechanism [11], and the effects of atmospheric delay [1,12]. These works have provided a solid theoretical basis for the development of phase enhancement and modelling algorithms used in MTInSAR, e.g., filtering [13,14], phase unwrapping [15–20], unbiased estimation of coherence [21,22], atmospheric mitigation [23–25], persistent scatterer (PS) and distributed scatterer (DS) selection and phase optimization [26–32]. Many of the algorithms have become routine functions in MTInSAR processing packages, either commercial or open-source.

As an illustration, Figure 1 shows a MTInSAR technical framework including some representative algorithms. Great accomplishments in the field of MTInSAR have been made on the selection of scatterers or pixels that can keep high phase quality over a certain period and the retrieval of deformation phase and topographic error from the original phase observations or enhanced/filtered phases of the selected points (PS + DS) (Figure 1).

Aiming to address the advances in InSAR imaging and data processing, we initiated this Special Issue and collected a total of 17 papers that cover a variety of topics, e.g., MTInSAR observation selection and enhancement, phase ambiguity estimation, atmospheric delay mitigation, advances in SAR imaging and applications. Their key innovations are summarized in the following sections.

check for updates

Citation: Zhang, L.; Lu, Z. Advances in InSAR Imaging and Data Processing—A Review. *Remote Sens.* **2022**, *14*, 4307. https://doi.org/10.3390/rs14174307

Received: 12 August 2022
Accepted: 29 August 2022
Published: 1 September 2022

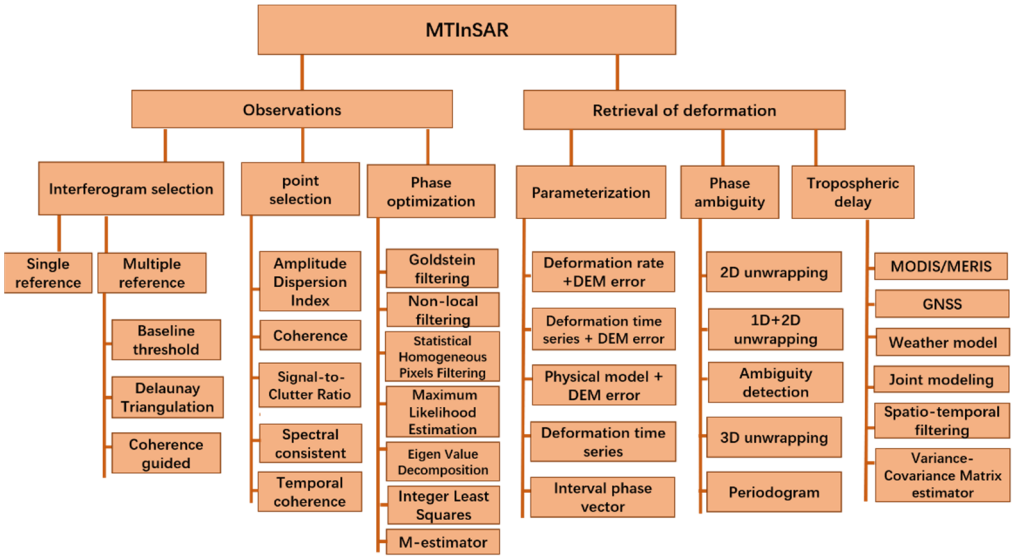

Figure 1. The technical framework of MTInSAR.

2. MTInSAR Observation Selection and Enhancement

The selection of proper observations (including interferograms and coherent points) is vital to a reliable MTInSAR processing (Figure 1). As a basic input of MTInSAR, both single-reference and multiple-reference interferogram stacks can be utilized. Once the interferograms are selected, the coherent points, both PS and DS pixels, are then identified. For the DS, as their phases suffer decorrelation to some extent, phase enhancement is usually conducted before they are used for signal retrieval.

In this Special Issue, there are four papers focusing on dealing with the decorrelation noise of MTInSAR observations. In [33], the normalized difference vegetation index (NDVI) value was explored to evaluate the decorrelation mechanism in vegetated areas. A multi-stage model was developed, which can quantitatively estimate the decorrelation noise induced by vegetation. A real-data test conducted in Hunan province, China, verified the performance of the proposed model. Since the NDVI dataset can be obtained globally from freely available optical satellite images, the proposed model can be further tested in more sites.

Following recent advances in phase optimization algorithm (POA), Li et al. proposed an adaptive weighted phase optimization algorithm based on the sigmoid model for DS [34]. In the proposed algorithm, more reasonable weights were assigned to pixels of different quality. Moreover, coherence bias correction based on the second-kind statistics and an efficient solution strategy based on eigenvalue decomposition were derived and applied to achieve optimal phase series retrieval. Therefore, it can efficiently reduce the negative influence of low-coherence pixels and improve the optimization performance.

To address the inherent limitation of sparse measurements in non-urban areas in the conventional coherent pixels technique InSAR (CPT-InSAR), an adaptive coherent distributed pixels selection method was integrated into the CPT-InSAR processing chain [35]. DS pixels were identified by classical statistical testing and their phases were also optimized by the joint use of the phase triangle algorithm (PTA) and Eigen decomposition-based maximum likelihood estimator of interferometric phase (EMI) [35].

Recent years have also seen the application of deep learning for phase noise reduction. In this Special Issue, Pu et al. developed an encoder–decoder network for accurate InSAR phase filtering [36]. Compared to the existing deep learning-based phase-filtering methods that are based on local neighboring pixels and local phase information, the proposed method utilized the encoder–decoder structure and nonlocal feature selection strategy. Experiments on both simulated and real InSAR data show that the proposed method significantly outperforms three traditional well-established methods [36].

3. Phase Ambiguity Estimation

Phase ambiguity behind the direct InSAR measurements (i.e., the wrapped phases) hinders us from retrieving the absolute deformation with respect to a reference point. Numerous algorithms have been developed to estimate the phase ambiguities, which were conducted either in the spatial domain or spatiotemporal domain. In this Special Issue, three papers contributed to this field. To improve the performance of the multi-baseline phase unwrapping (MBPU) algorithm over areas with low coherence based on conventional cluster analysis, Yuan et al. proposed to conduct the block-matching and 3D filtering (BM3D) algorithm before phase unwrapping and defined four different similarity measures to evaluate the filtering performance [37]. The work can serve as a reference when the BM3D algorithm is used in MBPU.

Zhang et al. contributed to this Special Issue with an adaptive square-root unscented Kalman filter phase unwrapping method aiming to tackle the challenges in regions with large phase gradients and high noise [38]. By combining a modified phase gradient estimation (PGE) algorithm and an adaptive square-root unscented Kalman filter, the proposed method has better accuracy and model robustness compared to the state-of-the-art, e.g., the minimum-cost flow algorithm (MCF) and statistical-cost network-flow algorithm (SNAPHU).

Mao et al. proposed another strategy to enhance the success rate of phase unwrapping in noisy areas where hierarchical networking and constrained adjustment were employed [39]. Both the simulated and real-data tests indicated that, compared with other traditional 2D phase unwrapping workflows, the proposed method can more accurately recover the phases of low-coherence regions.

4. Atmospheric Delay Mitigation

When penetrating through the atmosphere, radar waves can be delayed by water vapor in the tropospheric layer. Such a delay is sometimes clearly visible in an interferogram and serves as an error source in deformation retrieval. Mitigation of phases raised by atmospheric delay is challenging, as they could have a similar temporal behavior to non-linear deformation and their correlation scales vary from place to place in spatial domain. In this Special Issue, Liu et al. proposed a novel model-based method [40] to mitigate the atmospheric delay in the data collected by ground-based InSAR (GB-InSAR). Two experiments with different equipment over two study areas demonstrated that the proposed method can have a satisfactory performance on heterogenous atmospheric compensation in the azimuthal and horizontal directions.

5. Advances in SAR Imaging

Besides advances in InSAR data processing, this Special Issue also includes one paper on a novel imaging radar, i.e., wideband multiple-input-multiple-output (MIMO) radar [41]. MIMO radar utilizes the waveform diversity technique to synthesize a large aperture, which represents the largest difference from a generic GB-SAR. However, it is vulnerable to some inherent errors, e.g., element position error and inter-channel error. The paper proposed a method for estimating and compensating the array errors of wideband MIMO imaging radar based on multiple prominent targets. The in situ experiment demonstrated that the proposed method can improve the imaging performance of the wideband MIMO radar.

6. Applications

6.1. Geohazard Detection

It has long been recognized that, due to the dense vegetation, it is very challenging for the InSAR technique to detect slope movement over forested terrains, especially with current spaceborne radars which work on X-, C- and L-bands. Considering that longer waves have better penetration ability, Xu et al. experimented by using repeat-pass airborne P-band SAR data to detect geohazards over densely vegetated regions in Oregon and California (USA) [42]. The result shows that P-band interferograms have far better coherence

compared with L-band over densely vegetated areas, indicating that P-band InSAR could be a revolutionary tool for studying geohazards under dense forest canopies.

Besides the SAR wavelength, the processing strategy can also affect the performance of InSAR on geohazard identification over vegetated areas. Zhang et al. conducted a comparison between stacking and small baseline subset (SBAS) InSAR processing methods over a mountainous region in Southwestern China using Sentinel-1 images [43]. The results indicate that although stacking method may miss a few active slopes with small spatial scales, it outperforms SBAS over the study area and could be a fast and powerful method to qualitatively and effectively identify potential landslides in mountainous areas.

6.2. Deformation Mapping

InSAR has been proved as a promising tool for deformation mapping thanks to its unique abilities, e.g., wide coverage, fine resolution and high precision. Numerous successful applications have been conducted in the past several decades, where unprecedented measurements significantly enriched our understanding of the causal mechanism behind the events.

In this Special Issue, there are six papers that detailed InSAR applications in different fields. Qu et al. mapped the recent vertical crustal deformation of Weihe Basin (China) using Sentinel-1 and ALOS-2 images, revealing that vertical movement dominates the deformation of the Weihe Basin [44]. They also refined the fault traces using InSAR-derived displacement mapping, most of which are consistent with the existing inventory.

Bao et al. focused on ground deformation pattern analysis and evolution prediction of Shanghai Pudong International Airport [45], where Sentinel-1A images were processed by the Stanford method for persistent scatterers (StaMPS) package and the long short-term memory (LSTM) neural network was used for the short-term prediction of the deformation. The time-series observations and prediction results are expected to provide references for the airport expansion project to minimize ground subsidence and the impact to infrastructure.

Zhang et al. conducted underground goaf parameters estimation by cross-iteration with InSAR measurements [46]. Compared with conventional methods which are labor intensive, low efficiency and expensive, InSAR technology possesses unique advantages for goaf detection. They proposed a cross-iteration method for accurate inversion of underground goaf parameters. The reliability of the method was verified through simulation and real-data experiments.

Liao et al. investigated the ground subsidence of Yan'an, a western city in the loess plateau of China using Sentinel-1A time series images [47]. The spatial distribution characteristics and the time-series evolution trend of the subsidence over Yan'an New District (YAND) were retrieved. The results indicate that the YAND is relatively stable in general, with deformation rates mainly in the range of −10 to 10 mm/yr, while three significant subsidence funnels existed in the fill area, with a maximum subsidence rate of 100 mm/yr.

In [48], Yang et al. attempted to retrieve coseismic displacement associated with the 2016 Kumamoto earthquake from ALOS PALSAR-2 images acquired in both the right- and left-looking observation modes. As left-looking satellite SAR images were rare, their contribution to coseismic fault slip distribution should be evaluated. The authors concluded that the left-looking SAR data can complement the right-looking data in ground deformation mapping and enhance source model inversion. With the anticipated NASA-ISRO SAR (NISAR) satellite mission in early 2024, left-looking L-band SAR images will be globally available for Earth monitoring (https://nisar.jpl.nasa.gov/, accessed on 20 May 2022).

The Special Issue also included a paper on detecting rock glacier displacement in the Central Himalayas using MTInSAR [49]. To ensure a comprehensive measurement of rock glaciers, Zhang et al. evaluated the quality of all possible Sentinel-1 interferograms over the areas of interests and constructed a multi-baseline interferogram network according to coherence. They then applied a robust method to estimate the glacier displacements from the selected interferograms. The results indicate that the line-of-sight (LOS) deformation of rock glaciers in the central Himalayas ranged from −150 mm to 150 mm.

7. Conclusions

The recent increase in SAR satellites has resulted in a golden age of SAR data of various wavelengths and resolutions, providing important input for exploring multi-dimensional, multi-temporal InSAR analysis. The large amount of SAR data coupled with innovative spatial–temporal analyses are improving InSAR data processing methods. The advanced processing techniques then enable the extraction of geospatial information (especially deformation) at ultra-fine or extremely large scales, allowing for innovative applications on Earth monitoring. The papers in this Special Issue reflect the technical advances in decorrelation noise reduction, phase ambiguity estimation, atmospheric delay mitigation, and innovative applications in geohazard detection and deformation monitoring. There is no doubt that, equipped with innovative algorithms, the MTInSAR technique will play an important role in more and more exciting applications where big SAR data are turned into big insight.

Author Contributions: Conceptualization, Z.L. and L.Z.; formal analysis, L.Z.; writing—original draft preparation, L.Z.; writing—review and editing, Z.L.; supervision, Z.L.; funding acquisition, Z.L. and L.Z. All authors have read and agreed to the published version of the manuscript.

Funding: This work is funded in part by Natural Science Foundation of China (42174005) and in part by National Key R&D Program of China (2021YFC3000400) and the Shuler-Foscue Endowment at Southern Methodist University.

Conflicts of Interest: The authors declare no conflict of interest.

References

1. Hanssen, R. *Radar Interferometry: Data Interpretation and Error Analysis*, 1st ed.; Kluwer Academic Publishers: Dordrecht, The Netherlands, 2001.
2. Rosen, P.A.; Hensley, S.; Joughin, I.; Li, F.K.; Madsen, S.; Rodriguez, E.; Goldstein, R.M. Synthetic aperture radar interferometry. *Proc. IEEE* **2000**, *83*, 333–382.
3. Lu, Z.; Dzurisin, D. *InSAR Imaging of Aleutian Volcanoes: Monitoring a Volcanic Arc from Space*; Springer Praxis Books; Geophysical Sciences: Chicago, IL, USA, 2014.
4. Zhang, L.; Ding, X.L.; Lu, Z. Ground deformation mapping by fusion of multi-temporal interferometric synthetic aperture radar images: A review. *Int. J. Image Data Fus.* **2015**, *6*, 289–313. [CrossRef]
5. Li, F.; Goldstein, R.M. Studies of multi-baseline spaceborne interferometric synthetic aperture radars. *IEEE Trans. Geosci. Remote Sens.* **1990**, *28*, 88–97. [CrossRef]
6. Barber, B.C. The phase statistics of a multichannel radar interferometer. *Wave Random Media* **1993**, *3*, 257–266. [CrossRef]
7. Just, D.; Bamler, R. Phase Statistics of Interferograms with Applications to Synthetic Aperture Radar. *Appl. Opt.* **1994**, *33*, 4361–4368. [CrossRef]
8. Seymour, M.S.; Cumming, I.G. Maximum likelihood estimator for SAR interferometry. In Proceedings of the IGARSS, Pasadena, CA, USA, 8–12 August 1994; pp. 2272–2275.
9. Joughin, I.R.; Winebrenner, D.P.; Percival, D.B. Probability density functions for multilook polarimetric signatures. *IEEE Trans. Geosci. Remote Sens.* **1994**, *32*, 562–574. [CrossRef]
10. Touzi, R.; Lopes, A. Statistics of the Stokes Parameters and of the Complex Coherence Parameters in One-Look and Multilook Speckle Fields. *IEEE Trans. Geosci. Remote Sens.* **1996**, *34*, 519–531. [CrossRef]
11. Zebker, H.; Villasenor, J. Decorrelation in interferometric radar echoes. *IEEE Trans. Geosci. Remote Sens.* **1992**, *30*, 950–959. [CrossRef]
12. Treuhaft, R.N.; Lanyi, G.E. The effect of the dynamic wet troposphere on radio interferometric measurements. *Radio Sci.* **1987**, *22*, 251–265. [CrossRef]
13. Goldstein, R.M.; Werner, C.L. Radar interferogram filtering for geophysical applications. *Geophys. Res. Lett.* **1998**, *25*, 4035–4038. [CrossRef]
14. Sica, F.; Cozzolino, D.; Zhu, X.X.; Verdoliva, L.; Poggi, G. InSAR-BM3D: A Nonlocal Filter for SAR Interferometric Phase Restoration. *IEEE Trans. Geosci. Remote Sens.* **2018**, *56*, 3456–3467. [CrossRef]
15. Costantini, M. A Novel Phase Unwrapping Method Based on Network Programming. *IEEE Trans. Geosci. Remote Sens.* **1998**, *36*, 813–821. [CrossRef]
16. Usai, S. The use of man-made features for long time scale INSAR. In Proceedings of the IGARSS, Singapore, 3–8 August 1997.
17. Chen, C.W.; Zebker, H.A. Network approaches to two-dimensional phase unwrapping: Intractability and two new algorithms. *J. Opt. Soc. Am. A* **2000**, *17*, 401–414. [CrossRef]

18. Pepe, A.; Lanari, R. On the Extension of the Minimum Cost Flow Algorithm for Phase Unwrapping of Multitemporal Differential SAR Interferograms. *IEEE Trans. Geosci. Remote Sens.* **2006**, *44*, 2374–2383. [CrossRef]
19. Piyush Shanker, A.; Zebker, H. Edgelist phase unwrapping algorithm for time series InSAR analysis. *J. Opt. Soc. Am. A* **2010**, *27*, 605–612. [CrossRef]
20. Zhang, L.; Ding, X.L.; Lu, Z. Modeling the PSInSAR time-series without phase unwrapping. *IEEE Trans. Geosci. Remote Sens.* **2011**, *49*, 547–556. [CrossRef]
21. Jiang, M.; Ding, X.L.; Li, Z.W. Hybrid approach for unbiased coherence estimation for multitemporal InSAR. *IEEE Trans. Geosci. Remote Sens.* **2014**, *52*, 2459–2473. [CrossRef]
22. Jiang, M.; Guarnieri, A.M. Distributed scatterer interferometry with the refinement of spatiotemporal coherence. *IEEE Trans. Geosci. Remote Sens.* **2020**, *58*, 3977–3983. [CrossRef]
23. Liang, H.Y.; Zhang, L.; Ding, X.L.; Lu, Z.; Li, X. Toward Mitigating Stratified Tropospheric Delays in Multitemporal InSAR: A Quadtree Aided Joint model. *IEEE Trans. Geosci. Remote Sens.* **2019**, *57*, 291–303. [CrossRef]
24. Zebker, H. Accuracy of a Model-Free Algorithm for Temporal InSAR Tropospheric Correction. *Remote Sens.* **2021**, *13*, 409.
25. Li, Z.; Cao, Y.; Wei, J.; Duan, M.; Wu, L.; Hou, J.; Zhu, J. Time-series InSAR ground deformation monitoring: Atmospheric delay modeling and estimating. *Earth-Sci. Rev.* **2019**, *192*, 258–284. [CrossRef]
26. Ferretti, A.; Prati, C.; Rocca, F. Nonlinear subsidence rate estimation using permanent scatterers in differential SAR Interferometry. *IEEE Trans. Geosci. Remote Sens.* **2000**, *38*, 2202–2212. [CrossRef]
27. Hooper, A.; Segall, P.; Zebker, H. Persistent scatterer interferometric synthetic aperture radar for crustal deformation analysis, with application to Volcán Alcedo, Galápagos. *J. Geophys. Res.* **2007**, 112. [CrossRef]
28. Berardino, P.; Fornaro, G.; Lanari, R.; Sansosti, E. A new algorithm for surface deformation monitoring based on small baseline differential SAR interferograms. *IEEE Trans. Geosci. Remote Sens.* **2002**, *40*, 2375–2383. [CrossRef]
29. Ferretti, A.; Fumagalli, A.; Novali, F.; Prati, C.; Rocca, F.; Rucci, A. A New Algorithm for Processing Interferometric Data-Stacks: SqueeSAR. *IEEE Trans. Geosci. Remote Sens.* **2011**, *49*, 3460–3470. [CrossRef]
30. Cao, N.; Lee, H.; Jung, H.C. A phase-decomposition-based PSInSAR processing method. *IEEE Trans. Geosci. Remote Sens.* **2015**, *54*, 1074–1090. [CrossRef]
31. De Zan, F. Optimizing SAR Interferometry for Decorrelating Scatterers. Ph.D. Thesis, Politecnico di Milano, Milano, Italy, 2008.
32. Samiei-Esfahany, S. Exploitation of Distributed Scatterers in Synthetic Aperture Radar Interferometry. Ph.D. Thesis, Technische Universiteit Delft, Delft, The Netherlands, 31 May 2017.
33. Chen, Y.; Sun, Q.; Hu, J. Quantitatively Estimating of InSAR Decorrelation Based on Landsat-Derived NDVI. *Remote Sens.* **2021**, *13*, 2440. [CrossRef]
34. Li, S.; Zhang, S.; Li, T.; Gao, Y.; Zhou, X.; Chen, Q.; Zhang, X.; Yang, C. An Adaptive Weighted Phase Optimization Algorithm Based on the Sigmoid Model for Distributed Scatterers. *Remote Sens.* **2021**, *13*, 3253. [CrossRef]
35. Dong, L.; Wang, C.; Tang, Y.; Zhang, H.; Xu, L. Improving CPT-InSAR Algorithm with Adaptive Coherent Distributed Pixels Selection. *Remote Sens.* **2021**, *13*, 4784. [CrossRef]
36. Pu, L.; Zhang, X.; Zhou, L.; Li, L.; Shi, J.; Wei, S. Nonlocal Feature Selection Encoder–Decoder Network for Accurate InSAR Phase Filtering. *Remote Sens.* **2022**, *14*, 1174. [CrossRef]
37. Yuan, Z.; Chen, T.; Xing, X.; Peng, W.; Chen, L. BM3D Denoising for a Cluster-Analysis-Based Multibaseline InSAR Phase-Unwrapping Method. *Remote Sens.* **2022**, *14*, 1836. [CrossRef]
38. Zhang, Y.; Zhang, S.; Gao, Y.; Li, S.; Jia, Y.; Li, M. Adaptive Square-Root Unscented Kalman Filter Phase Unwrapping with Modified Phase Gradient Estimation. *Remote Sens.* **2022**, *14*, 1229. [CrossRef]
39. Mao, W.; Wang, S.; Xu, B.; Li, Z.; Zhu, Y. An Improved Phase Unwrapping Method Based on Hierarchical Networking and Constrained Adjustment. *Remote Sens.* **2021**, *13*, 4193. [CrossRef]
40. Liu, J.; Yang, H.; Xu, L.; Li, T. Novel Model-Based Approaches for Non-Homogenous Atmospheric Compensation of GB-InSAR in the Azimuth and Horizontal Directions. *Remote Sens.* **2021**, *13*, 2153. [CrossRef]
41. Zhao, Z.; Tian, W.; Deng, Y.; Hu, C.; Zeng, T. Calibration Method of Array Errors for Wideband MIMO Imaging Radar Based on Multiple Prominent Targets. *Remote Sens.* **2021**, *13*, 2997. [CrossRef]
42. Xu, Y.; Lu, Z.; Kim, J.-W. P-Band InSAR for Geohazard Detection over Forested Terrains: Preliminary Results. *Remote Sens.* **2021**, *13*, 4575. [CrossRef]
43. Zhang, L.; Dai, K.; Deng, J.; Ge, D.; Liang, R.; Li, W.; Xu, Q. Identifying Potential Landslides by Stacking-InSAR in Southwestern China and Its Performance Comparison with SBAS-InSAR. *Remote Sens.* **2021**, *13*, 3662. [CrossRef]
44. Qu, F.; Zhang, Q.; Niu, Y.; Lu, Z.; Wang, S.; Zhao, C.; Zhu, W.; Qu, W.; Yang, C. Mapping the Recent Vertical Crustal Deformation of the Weihe Basin (China) Using Sentinel-1 and ALOS-2 ScanSAR Imagery. *Remote Sens.* **2022**, *14*, 3182. [CrossRef]
45. Bao, X.; Zhang, R.; Shama, A.; Li, S.; Xie, L.; Lv, J.; Fu, Y.; Wu, R.; Liu, G. Ground Deformation Pattern Analysis and Evolution Prediction of Shanghai Pudong International Airport Based on PSI Long Time Series Observations. *Remote Sens.* **2022**, *14*, 610. [CrossRef]
46. Zhang, W.; Shi, J.; Yi, H.; Zhu, Y.; Xu, B. Underground Goaf Parameters Estimation by Cross-Iteration with InSAR Measurements. *Remote Sens.* **2021**, *13*, 3204. [CrossRef]
47. Liao, M.; Zhang, R.; Lv, J.; Yu, B.; Pang, J.; Li, R.; Xiang, W.; Tao, W. Subsidence Monitoring of Fill Area in Yan'an New District Based on Sentinel-1A Time Series Imagery. *Remote Sens.* **2021**, *13*, 3044. [CrossRef]

48. Yang, Y.-H.; Chen, Q.; Xu, Q.; Zhao, J.-J.; Hu, J.-C.; Li, H.-L.; Xu, L. Comprehensive Investigation of Capabilities of the Left-Looking InSAR Observations in Coseismic Surface Deformation Mapping and Faulting Model Estimation Using Multi-Pass Measurements: An Example of the 2016 Kumamoto, Japan Earthquake. *Remote Sens.* **2021**, *13*, 2034. [CrossRef]
49. Zhang, X.; Feng, M.; Zhang, H.; Wang, C.; Tang, Y.; Xu, J.; Yan, D.; Wang, C. Detecting Rock Glacier Displacement in the Central Himalayas Using Multi-Temporal InSAR. *Remote Sens.* **2021**, *13*, 4738. [CrossRef]